Ocean Engineering 269 (2023) 113554

Contents lists available at ScienceDirect

Ocean Engineering

journal homepage: www.elsevier.com/locate/oceaneng

Experimental study on the dynamic response of a silty seabed under waves

Lihua Wang [a], Jinfeng Zhang [a,b,*], Dong-Sheng Jeng [c,d], Qinghe Zhang [a], Tongqing Chen [a]

[a] State Key Laboratory of Hydraulic Engineering Simulation and Safety Tianjin University, Tianjin, 300072, China
[b] Key Laboratory of Earthquake Engineering Simulation and Seismic Resilience of China Earthquake Administration, Tianjin University, Tianjin, 300350, China
[c] School of Engineering & Built Environment, Griffith University Gold Coast Campus, Queensland, 4222, Australia
[d] Qingdao Technology Innovative Center for Ocean Dynamic Environmental Simulations, College of Civil Engineering, Qingdao University of Technology, Qingdao, 266033, China

ARTICLE INFO

Handling Editor: A.I. Incecik

Keywords:
Experiments
Wave flume
Wave-induced pore pressure
Suspended sediment concentration
Phase lag
Scour
Liquefaction

ABSTRACT

Scouring and liquefaction of silty seabeds under waves have been recognized as two major modes of the seabed instability around marine structures. A series of wave experiments were conducted to investigate the wave-induced dynamic response in a silty seabed. The seabed was composed of light sand with and without geotextile covering under various wave conditions. When the seabed was not covered with geotextile, the seabed was liquefied under the action of waves, accompanied by sediment incipience and suspension. The results show that with increasing wave height, the seabed develops a series of processes such as sand ripples, ripple attenuation, sheet flow and seabed liquefaction. After seabed liquefaction occurs, an upward force gradient of the accumulated pore pressure is generated, which increases the suspended sediment concentration near the bottom and further enhances the scour of the seabed. When it is scoured, the sediment particles are continuously removed, and the stress in the soil is released, which intensifies seabed liquefaction. When the seabed is covered with geotextile, the concentration of suspended sediment near the bottom is zero. The maximum liquefaction depth of the seabed decreases along with the development rate of the liquefaction depth. The amplitude of the pore water pressure in the seabed decreases by approximately 5%–20% and seabed liquefaction is reduced. Experimental results clarify that liquefaction and scour promote each other.

1. Introduction

Waves are one of the important environmental loadings acting on offshore structures and seabed in the marine environment. Under waves, the effective normal stress between the individual grains in the seabed is reduced, which may further lead to seabed liquefaction and result in the instability of offshore structures (Chung et al., 2006; Puzrin et al., 2010; Sumer, 2014). More than 70% of the seabed in coasts and offshore areas in China is composed of silt and soft clay (Ding et al., 2013). The silty seabed under waves is obviously different from the sandy seabed. Silt has low shear strength and adhesion between fine particles. The liquefaction resistance decreases with increasing fine particle content (Gobbi et al., 2022). Furthermore, the liquefaction criterion for a sandy seabed may not be applicable in silty soil seabeds (Jeng and Seymour., 2007; Li et al., 2014). Liquefaction of silty seabeds is more harmful. For example, thousands of buildings, city lifelines and infrastructure have been damaged due to liquefaction of silty seabeds (Cubrinovski et al., 2011). Therefore, it is important to investigate the dynamic response of silty seabeds under waves.

For the dynamic response of a silty seabed under waves, some experiments have been carried out. Among these, Sumer and his coworkers (Sumer et al., 1999, 2006, 2012, Kirca et al., 2013) conducted a series of wave experiments and concluded that when the wave height exceeded a certain value and the accumulated pore pressure reached the initial mean effective normal stress, the seabed liquefied. At this critical state, the seabed suddenly changed from the solid phase to the fluid phase. Later, Tong et al. (2018) concluded that the pore pressure response was different at the surface and deep layer of the seabed, and the wave attenuation caused by liquefaction was dramatic. Xu et al. (2021) and Ren et al. (2020) observed that seabed liquefaction started from the surface layer and gradually developed downward through field observations and wave flume tests. In the process of liquefaction, three typical stages were included, including quasi-elastic, intensive build-up, and continuous liquefaction stages (Li et al., 2022). After seabed liquefaction, the soil strength increased, the water content decreased, and the compactness of the soil increased (Wen et al., 2020). In addition, a lot of

* Corresponding author. State Key Laboratory of Hydraulic Engineering Simulation and Safety Tianjin University, Tianjin, 300072, China.
E-mail address: jfzhang@tju.edu.cn (J. Zhang).

https://doi.org/10.1016/j.oceaneng.2022.113554
Received 31 October 2022; Received in revised form 18 December 2022; Accepted 23 December 2022
Available online 3 January 2023
0029-8018/

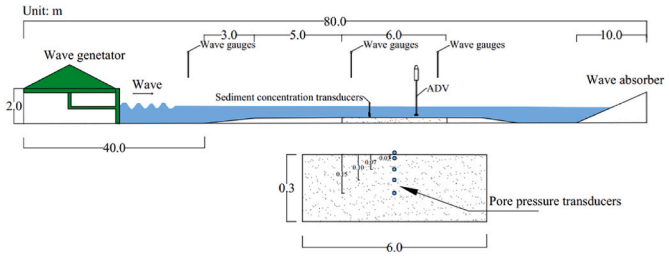

Fig. 1. Configuration of the wave experiment setup.

parametric study were conducted to investigate the effects of the soil and wave characteristics to liquefaction (Hu et al., 2020; Liu and Jeng, 2015; Sui et al., 2022; Xu et al., 2022). These experiments revealed the forces and deformations inside the seabed without considering other phenomena associated with liquefaction, such as incipient sediment motion and seabed scour.

In fact, there are several failure modes of a silty seabed under wave loading, such as scour, liquefaction, shear failure, etc., and they interact. Qi and Gao (2014) and Takegawa et al. (2016) concluded that the excess pore pressure and liquefaction induced by waves would aggravate the scour and affect its profile. Zhang et al. (2018) and Dong et al. (2022) also concluded that wave-induced seabed fluidization and liquefaction promoted sediment resuspension of the seabed. The scour of the seabed changed the sediment transport near the bottom and affected the liquefaction process of the seabed under waves. However, seabed erosion, seabed liquefaction, seepage instability and shear failure caused by waves are the simultaneous overall response of the seabed (Peng et al., 2017). How seabed liquefaction and scour interact has not yet been clarified. This is particularly important for the design of marine infrastructures.

In this study, a series of wave experiments for the dynamic response of a silty seabed were conducted. Two conditions were designed for the experiment. One was to consider the impact of seabed scour, and the other was to lay geotextiles to prevent seabed scour. The changes in pore water pressure and suspended sediment concentration near the bottom of the seabed were analyzed. The experimental setup is described in Section 2, while the dynamic response of the seabed with and without seabed scour are described in Section 3 and Section 4, respectively. The discussion and conclusions are summarized in Sections 5 and 6.

2. Experiments

2.1. Wave flume and instrumentation

The experiments were conducted in the wave flume of the State Key Laboratory of Hydraulic Engineering Simulation and Safety, Tianjin University, as shown in Fig. 1. The flume was 80.0 m × 2.0 m × 2.0 m. The test section was located at the middle and rear of the flume, in which the seabed was 6.0 m × 2.0 m × 0.30 m. A block stone slope was laid at the end as a wave elimination area to prevent reflected waves. To ensure the wave attenuation effect, the "3-point method" (Mansard and Funke, 1980) was adopted to deploy the wave gauges and the calculated maximum wave reflection coefficient was 2.15%. In the experiments, an ADV manufactured by the Sontek company was used to measure the horizontal velocity of water near the bed surface. The measurement range was ±0–3 m/s with an accuracy of ±0.5%, and the sampling frequency was set to 50 Hz for all experiments. A multichannel sediment concentration measurement instrument based on an optical fiber sensor was used to measure the near bottom suspended sediment concentration. The measurement range was 150 kg/m^3 with an accuracy of ±5%, and the sampling frequency was set to 20 Hz. The YY-2 pore water pressure gauge was fixed to measure the pore water pressures in the seabed, which was developed by the Nanjing Academy of Hydraulic Sciences. The measurement range was 35 kPa, the sampling accuracy

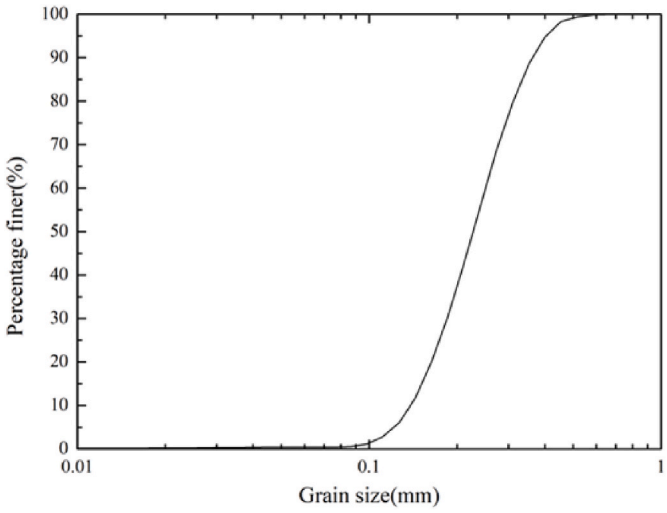

Fig. 2. Grain distribution of sand used in the wave experiments.

was 0.2% FS, and the sampling frequency was set to 20 Hz. The data were controlled and collected by computer. A high-speed camera was erected outside the sidewall of the flume to record the phenomenon.

Light sand with $d_{50} = 0.24$ mm was selected as the experimental sand. The specific weight of sediment grains is 1.195, and the porosity $n = 0.42$. The particle size distribution is shown in Fig. 2.

2.2. Wave conditions

The wave conditions are summarized in Table 1. The wave with $d =$ 62 cm, $H = 9.8$ cm, and $T = 1.26$ s is obtained according to the actual wave conditions in the Dafeng area, Jiangsu Province. To study the influence of wave parameters, a series of waves with wave heights of $H =$ 3–14 cm and periods of $T = 1.1$ s–1.7 s was set. The water depth above the seabed is $d = 62$ cm in all cases. In the table, U_m is the maximum velocity of water particles at the bottom of the water. U_{fm} is the maximum friction velocity, $U_{fm} = \sqrt{\frac{f_w}{2}}U_m$, in which f_w is the wave friction coefficient, $f_w = \frac{2}{\sqrt{\mathrm{Re}}}$ and $\mathrm{Re} = \frac{aU_m}{\nu}$, and a is the amplitude of the orbital motion of water particles at the bottom. θ is the Shields parameter, $\theta = \frac{U_{fm}^2}{g(s-1)d_{50}}$, in which g is the acceleration due to gravity and s is the specific gravity of sediment grains. According to Le Méhauté (1976), the waves are Stokes 2-order and Stokes 3-order waves (Fig. 3). Fig. 4 shows the comparison results between the experimental wave surface of $H =$ 9.8 cm and the theoretical value of the Stokes 2nd-order wave, which are in good agreement. Each test was conducted three times to ensure the accuracy of the test data.

2.3. Seabed conditions

Usually, in the experiments in the wave flume of the seabed dynamics, the hydrodynamic conditions were reduced compared to the actual conditions, and then the sand used in the seabed was prototype sand (i.e., no reduced scale) (Sumer et al., 1999, 2006, 2012, Kirca et al., 2013; Xu et al., (2021). Ren et al. (2020). Qi and Gao (2014)). Therefore, the seabed composed of prototype sand cannot be liquefied under very small hydrodynamic conditions. In our study, light model sand with a density of 1195 kg/m^3 and a median particle size of 0.24 mm was used. According to the similarity of starting and settling, the liquefaction process of the seabed under waves was investigated. In addition, the scour and liquefaction phenomenon of the seabed were difficult to distinguish in the previous tests. Therefore, the geotextile was laid on the seabed surface to prevent incipient sediment motion and represents the innovation of our experiment. After testing, a geotextile of 100 g/m^2

Table 1
Test conditions. The water depth above the seabed is 62 cm in all cases.

Test no.	Wave height H (cm)	Wave period T (s)	Wavelength L (m)	Maximum value of orbital velocity at the bed; Measured U_m (cm/s)	Maximum value of friction velocity U_{fm} (cm/s)	Grain Reynolds number dU_{fm}/ν	Shields parameter θ	Ursell number	Liquefaction? Yes/No
Case 1	3	1.26	2.31	3.0	0.80	1.92	0.14	0.67	No
Case 2	5	1.26	2.31	5.0	1.03	2.48	0.23	1.12	No
Case 3	6	1.26	2.31	5.7	1.13	2.72	0.28	1.34	No
Case 4	7	1.26	2.31	6.5	1.22	2.93	0.33	1.57	No
Case 5	8	1.26	2.31	7.8	1.31	3.14	0.37	1.79	No
Case 6	9.8	1.26	2.31	9.2	1.45	3.47	0.46	2.19	Yes
Case 7	12	1.26	2.37	11.7	1.64	3.93	0.59	2.83	Yes
Case 8	14	1.26	2.39	13.3	1.78	4.28	0.69	3.36	Yes
Case 9	9.8	1.1	1.85	6.7	1.29	3.09	0.36	1.41	No
Case 10	9.8	1.5	3.02	13.0	1.58	3.80	0.55	3.75	Yes
Case 11	9.8	1.7	3.59	13.4	1.63	3.91	0.60	5.30	Yes

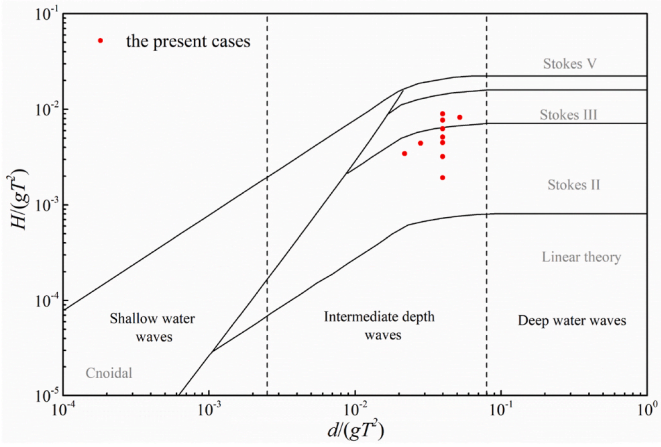

Fig. 3. Range of application of various wave theories.

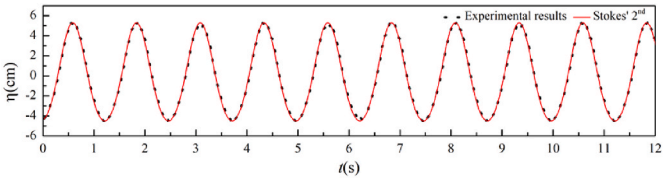

Fig. 4. Comparison of wave-surface time series (Case 6). The black dots are the experimental results, and the red solid line is the theoretical result of 2nd-order Stokes wave theory. (For interpretation of the references to colour in this figure legend, the reader is referred to the Web version of this article.)

Fig. 5. Seabed without geotextiles.

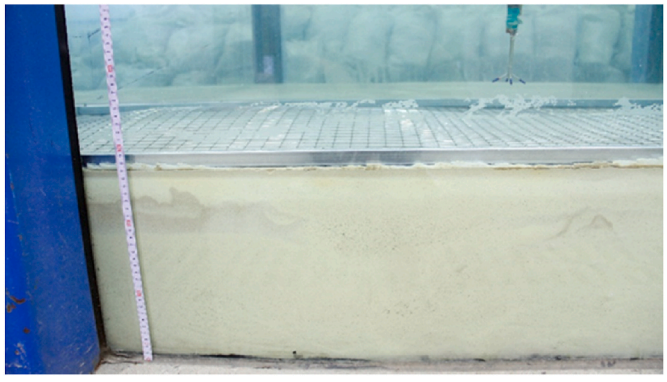

Fig. 6. The geotextiles and metal screens on the seabed surface.

with a thickness of 1 mm was chosen, and the strength of this geotextile ensured that it would not be torn by the water but allow the water penetrating well. The geotextiles were laid on the seabed surface, and metal screens were laid as fixed measures (Figs. 5 and 6). The water can penetrate the geotextiles well, but the sediment particles cannot pass through which prevents seabed scour and does not affect the dynamic response inside the seabed. To verify whether the geotextile affects the water seepage, taking the wave of $H = 9.8$ cm as an example, the pressure gauges were set up above and below the geotextile. The measured results are shown in Fig. 7. The figure shows that the geotextile can penetrate the water well and will not affect the dynamic

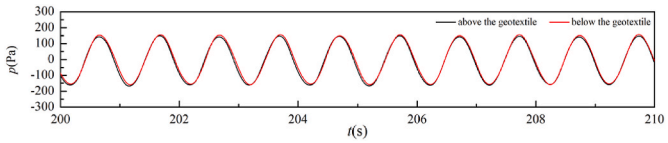

Fig. 7. The water pressure above and below the geotextile. The black and red lines are the measurement results above and below the geotextile, respectively. (Case 6). (For interpretation of the references to colour in this figure legend, the reader is referred to the Web version of this article.)

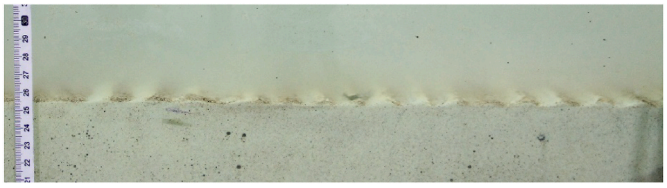

Fig. 8. Ripples on the bed with a width of 2–3 cm and a height of 2 mm (Case 3).

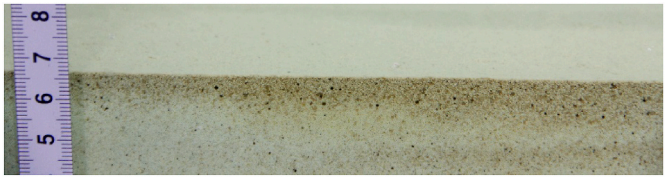

Fig. 9. Sheet flow with a height of 10–15 mm and the sorted grains on the bed (Case 5).

response in the bed.

3. Dynamic response with seabed scour

3.1. Experimental phenomenon

Under the action of water depth of 62 cm and period of 1.26 s, with the increase in loading wave height, the seabed sediment experiences the process from sediment incipient to ripple development, ripple attenuation, sheet flow and liquefaction. In Case 1, the sediment is not incipient. In Case 2, the sediment is incipient, and ripples appear, with a width of 2–3 cm and a height of 2 mm. In Case 3, the water begins to be turbid, the sediment is suspended, and sand ripples develop, with a width of 2–3 cm and a height of 3–4 mm (Fig. 8). In Case 4, the finer sediment is suspended in the upper water body, and the ripples are attenuated. Furthermore, the width change is not obvious, still approximately 2–3 cm, and the height is 2 mm. In Case 5, the ripples disappear, and the sediment, with a height of 10–15 mm on the surface of the seabed, moves in layers with the waves called sheet flow. After loading the waves for 30 min, the sediment in the sheet flow layer is obviously sorted, the fine particles move upward, and the coarser particles sink (Fig. 9).

In Case 6, the seabed is liquefied (based on visible observations), the sediment is suspended to the water surface, and the water body is turbid. Here, the excess pore pressures at different depths in the seabed are shown in Fig. 15 and the seabed is also liquefied according to the criterion of liquefaction (Jeng, 1997; Sumer et al., 2012). At the initial stage of wave loading, the liquefaction depth of the seabed developed rapidly. After approximately 4 min, the liquefaction depth reached a maximum value of 15 cm, which was captured by the high-speed camera. Then, the liquefaction depth gradually decreased. After approximately 30 min, the liquefaction depth decayed to 7–8 cm. After 60 min, the seabed was no longer liquefied, and the compactness increased. The

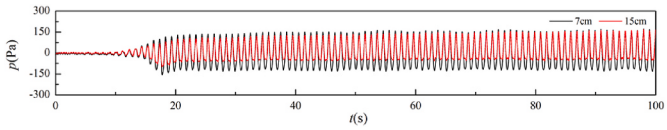

Fig. 10. Excess pore water pressure at the initial stage of wave action (Case 6).

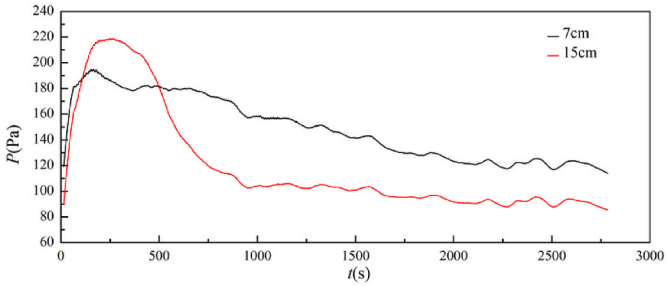

Fig. 11. Peak value of excess pore water pressure within 60 min (Case 6).

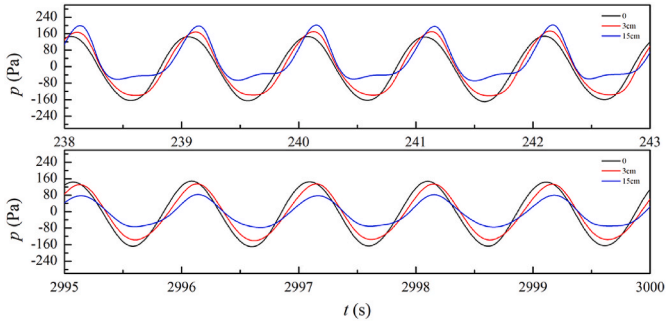

Fig. 12. The pore water pressure on the bed surface, and 3 cm, 15 cm below it after 4 min and 60 min of wave action (Case 6).

height of the sheet flow layer increased first and then decreased with wave loading. The maximum depth was approximately 2 cm and occurs 4 min after wave loading, which is consistent with the maximum liquefaction depth.

In Cases 7 and 8, the maximum liquefaction depths of seabed were 16 cm and 17 cm, respectively, both of which occurred approximately 4 min in the initial stage of wave loading. After approximately 30 min, the liquefaction depth decayed to approximately 12 cm, and after 60 min, the liquefaction depth decayed to approximately 9 cm, and the seabed compactness increased.

In Case 9, there were no ripples on the seabed surface, and the sediment, with a height of 5 mm on the seabed surface, was active and moved back and forth with waves. In Cases 10 and 11, the seabed liquefied. The maximum liquefaction depth was 17 cm. After 60 min, the liquefaction depth decayed to 9 cm.

3.2. Pore pressures in the seabed

Taking Case 6 as an example, the pore water pressure at 7 cm and 15 cm below the seabed surface at the initial stage is shown in Fig. 10, and the peak value of the pore pressure is shown in Fig. 11. The pore water pressure accumulates obviously at the beginning, and the accumulation is more obvious with increasing seabed depth. According to the liquefaction criteria, under the action of waves, when the excess pore water pressure at a certain point in the seabed is greater than the pressure of the overlying soil at that point, the seabed will be liquefied (Sumer et al., 2006). After 4 min of wave action, the cumulative value of pore water pressure at 15 cm below the bed reaches the maximum. Currently, the

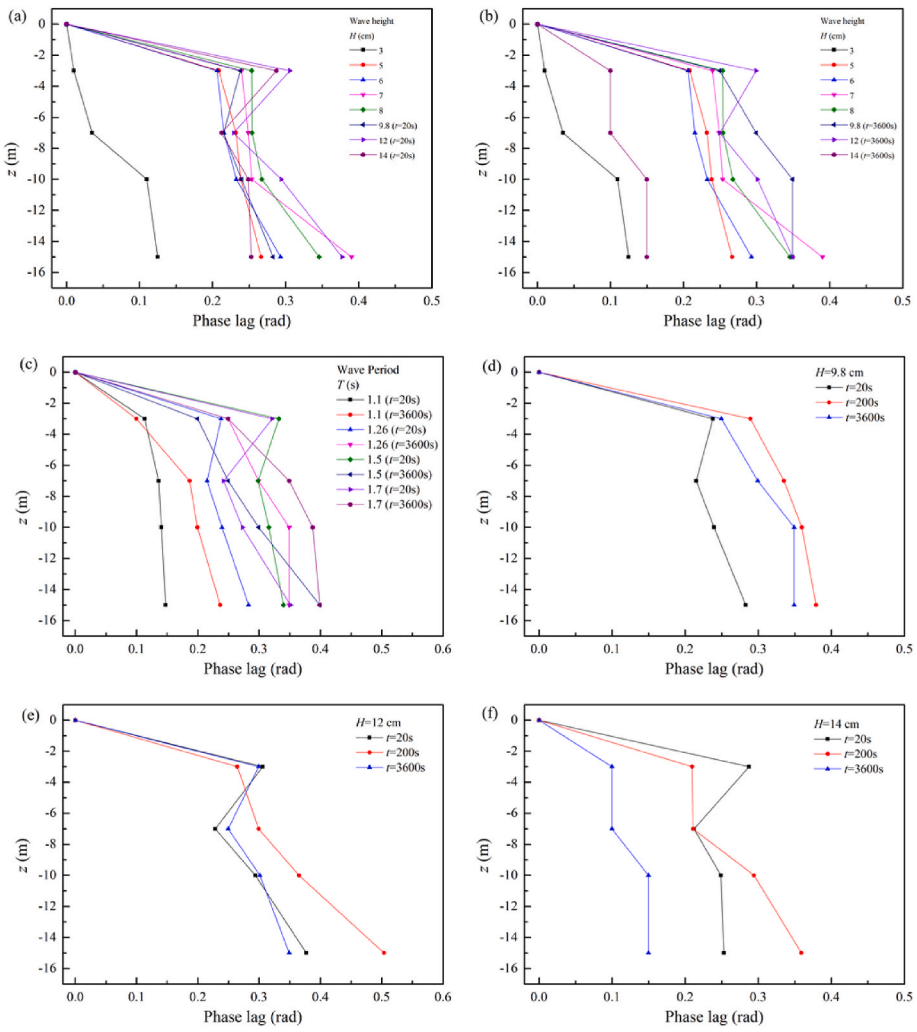

Fig. 13. Phase lag of pore water pressure at different depths in the seabed. (a) At the initial 20 s of wave loading (Cases 1–8). (b) After 1 h of wave loading (Cases 1–8). (c) At the initial stage of liquefaction ($t = 20$ s) and after 3600 s of wave loading (Cases 9–11). (d) After different wave loading times (Case 6). (e) After different wave loading times (Case 7). (f) After different wave loading times (Case 8).

average excess pore pressure at 7 cm and 15 cm below the seabed is 66 Pa and 146 Pa, respectively. Based on the initial effective stress at these two locations being 49 and 105 Pa, the seabed currently reaches the maximum liquefaction depth, which is consistent with the observation results.

The pore water pressure on the bed surface, and 3 cm, 15 cm below it after 4 min and 60 min of wave action is shown in Fig. 12. When the wave action lasts for 4 min, the liquefaction depth is a maximum of 15 cm. After 60 min, the seabed is no longer liquefied. At the initial stage of the wave action, the pore water pressure in the liquefaction area increases along the depth, and the pore water pressure curve is no longer regular. The liquefied seabed manifests as fluid with greater density than water, and the pore water pressure response is accompanied by the phase difference. After 60 min, the seabed compactness increases, no longer liquefies, the pore water pressure decays along the depth, and its phase lag along the depth decreases compared with the liquefaction.

The phase lag of pore water pressure at different depths in the seabed and the wave pressure at the seabed surface is shown in Fig. 13. Before seabed liquefaction, the phase lag value of pore water pressure at different depths did not change with time. After seabed liquefaction, the phase lag value changed with the loading wave time. The phase lag value of the initial 20 s of wave loading is shown in Fig. 13(a). Before incipient sediment motion, the phase lag was very small. Before seabed liquefaction, the phase lag increased with depth; it increased rapidly on the seabed surface, and then the rate of increase decreased with depth. With increasing wave height and wave period, the phase lag in the seabed became obvious (Fig. 13(a)–(c)). At the initial 20 s of wave loading, liquefaction developed downward; in the liquefaction area, the phase lag value was greatly increased compared with before liquefaction; in the non-liquefaction area deep in the seabed, the phase lag value does not change significantly. After 1 h of wave loading, the seabed compactness increased, which was also observed in Wen's experiments (Wen et al., 2020). The phase lag gradually disappeared with increasing damping in the seabed, which is consistent with the theoretical results derived by Okusa (1985).

To better understand the influence of liquefaction on the lag of the pore pressure response in the seabed, the results of phase lag at different depths at the initial stage of liquefaction ($t = 20$ s), at the time when liquefaction developed to the maximum depth ($t = 200$ s) and after 3600 s of wave loading are shown in Fig. 13(d)–(f). At a certain depth in the seabed, the phase lag after liquefaction was greater than that before liquefaction, and the phase lag inside the liquefaction area also increased with depth. After 60 min of wave loading, the density of the seabed increased, the higher the wave height was, the more obvious the compaction effect, and the smaller the phase lag value which was different from the conclusion obtained in the non-liquefied seabed (Li and Gao, 2022).

Comparing the phase results under the action of waves with different

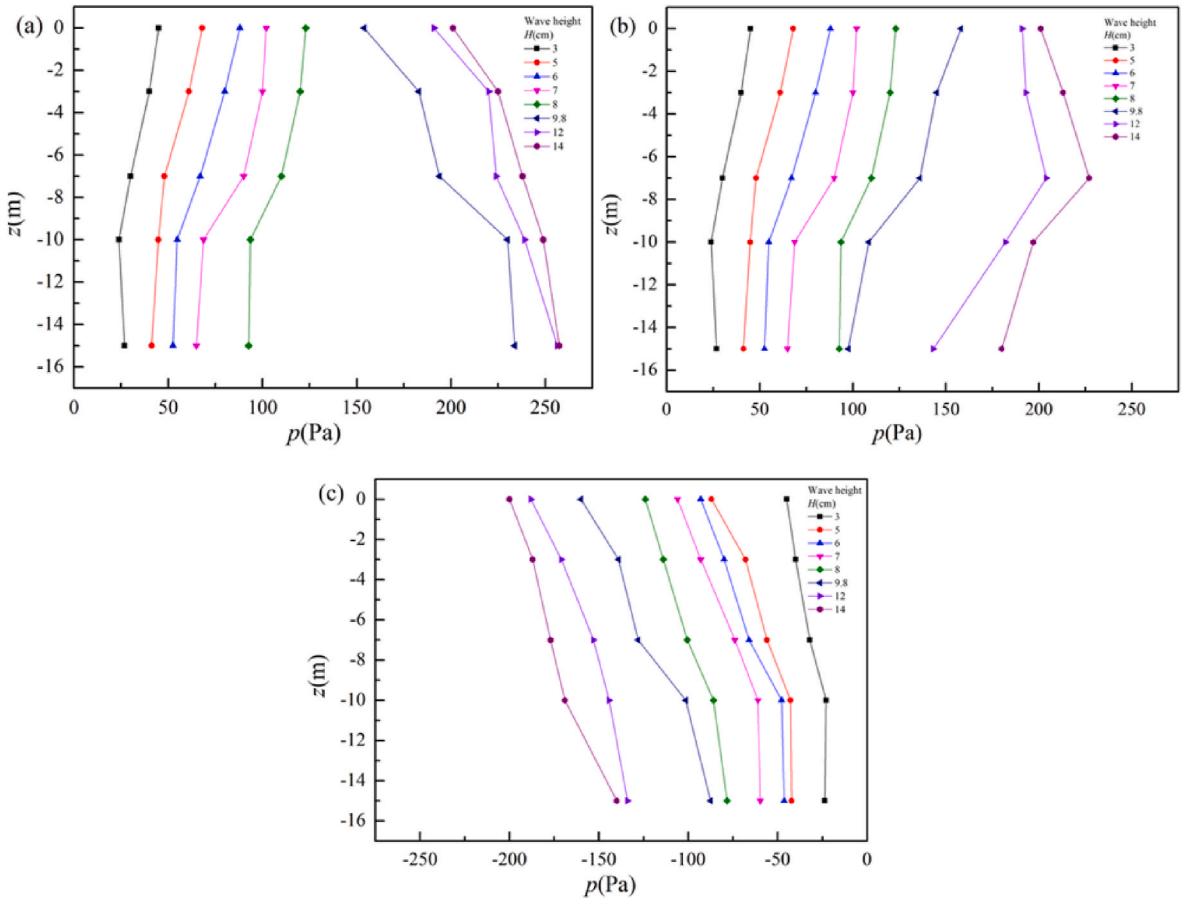

Fig. 14. Variation in pore water pressure amplitude with wave height at different depths in the seabed (a) Amplitude under the wave crest at the maximum accumulated pore water pressure ($t/T = 188$). (b) Amplitude of pore water pressure under the wave crest after 60 min of wave action ($t/T = 2857$) (c) Minimum pore water pressure under the wave trough.

wave heights and periods, the influence of periods on the phase lag in the seabed is smaller than that of wave heights.

The pore water pressure amplitude under wave action of a series of wave heights at the initial stage and after 60 min is shown in Fig. 14 and Table 2-Table 3. The amplitude of the pore water pressure increased with increasing wave height and increased significantly on the surface. The effective stress and average excess pore water pressure at different depths of the seabed in Cases 6–8 are shown in Fig. 15. When the wave height was less than 9.8 cm, the seabed was not liquefied, the pore water pressure decayed along the depth, and the deceleration rate gradually decreased. When the wave height was greater than or equal to 9.8 cm, the average excess pore pressure in the seabed was greater than the initial effective stress (Sumer et al., 2012), the seabed was liquefied, and the effective stress in the soil was 0. With the periodic movement of waves, it is shown as a fluid with a density greater than water, and the pore water pressure amplitude gradually increased along the depth direction (Fig. 14-(a), Fig. 15); After 60 min of wave action (Fig. 14-(b)), in Case 6, the seabed compactness increased, the porosity decreased, the permeability coefficient decreased, the soil strength increased, the seabed was no longer liquefied, and the pore water pressure amplitude decreased with increasing depth. In Case 7 and Case 8, the liquefaction depth decreased, and the pore water pressure amplitude increased with depth in the still liquefied area. In the no longer liquefied area, the pore water pressure amplitude decreased with the depth. Under the action of the wave trough (Fig. 14-(c) and Table 4), the pore water pressure was negative, decayed along the depth direction, and the seabed was pulled instantaneously.

The maximum and minimum pore pressure under wave action of a series of wave periods at the initial stage and after 60 min is shown in Fig. 16 and Table 5-Table 7. The pore water pressure increased with increasing period. When $T = 1.1$ s, the seabed was not liquefied. When T $\geq$ 1.26 s, the seabed was liquefied. The amplitude of the pore water pressure in the liquefaction area increased with depth. After 60 min of wave loading, the seabed compactness increased, the pore water pressure decreased with depth, and the greater the wave period was, the more obvious the compaction effect (see Table 6).

3.3. Near-bottom suspended sediment concentration

Suspended sediment concentration is an important environmental index for silty coasts. Under the combined action of waves and tidal currents, sediment sedimentation and resuspension occur, and the concentration of suspended sediment in the water body changes accordingly. The variation in suspended sediment concentration is of great significance to seabed scour and seabed instability.

In Case 6-Case 8, the velocity amplitude at the bed increased with increasing load wave height (Table 1). The sediment on the bed undergoes a process from threshold to the development of sand ripples, sheet flow, and suspension, which is accompanied by the intensification of sediment erosion on the bed.

The near-bottom suspended sediment concentration under the action of each wave height was measured, and the results are shown in Table 8. The measured concentration results and the theoretical results derived from Nielsen (1992), Zuo et al., (2019) and Xia et al. (2011) are shown in Fig. 17. Before liquefaction, the measured value is in good agreement with the theoretical value. The measured value after liquefaction was much larger than the theoretical value, which can be inferred to be due to the failure to consider the influence of seabed liquefaction in the

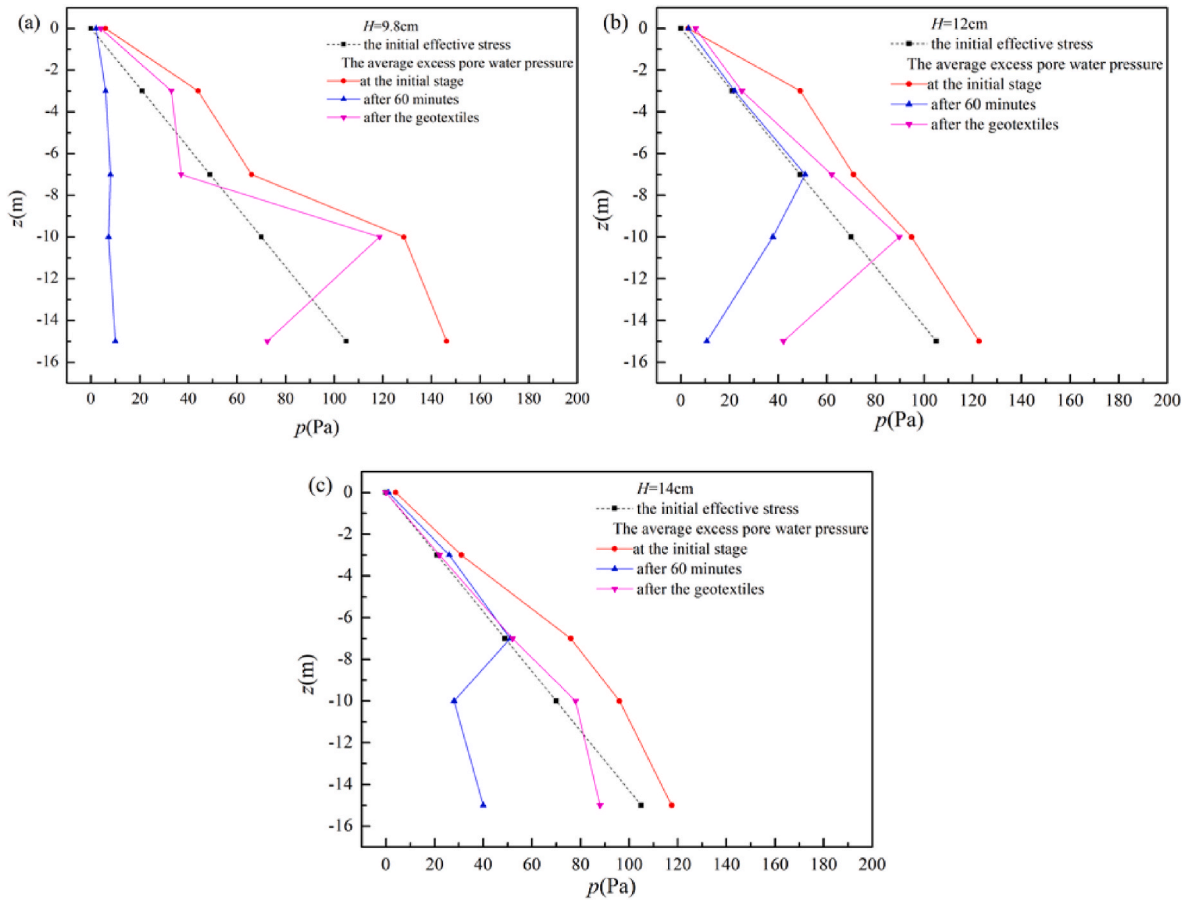

Fig. 15. The initial normal effective stress and the average excess pore water pressure at the initial stage, and $t = 60$ min under the conditions without geotextile covering. Then, the pore water pressure after geotextile covering (Cases 6–8).

Table 2
Maximum pore water pressure under the wave crest at different depths in the seabed at the initial stage of wave action (Pa) ($d = 62$ cm, $T = 1.26$ s).

z(cm) / H(cm)	3	5	6	7	8	9.8	12	14
0	45	68	88	102	123	154	191	201
−3	40	61	80	100	120	183	220	225
−7	30	48	67	90	110	194	224	238
−10	24	45	55	69	94	230	239	249
−15	27	41	53	65	93	234	256	258

Table 3
Maximum pore water pressure under the wave crest at different depths in the seabed after 60 min of wave action (Pa) ($d = 62$ cm, $T = 1.26$ s).

H(cm) / z(cm)	3	5	6	7	8	9.8	12	14
0	45	68	88	102	123	158	191	201
−3	40	61	80	100	120	145	193	213
−7	30	48	67	90	110	136	204	227
−10	24	45	55	69	94	109	182	197
−15	27	41	53	65	93	98	143	180

theoretical formula. The near bottom suspended sediment concentration increased with wave height. Before the occurrence of seabed liquefaction, the suspended sediment near the bottom increased slowly with wave height. After seabed liquefaction, the suspended sediment concentration increased sharply. It can be concluded that wave-induced seepage force and liquefaction have a significant role in promoting the suspended sediment concentration.

Table 4
Minimum pore water pressure at different depths of seabed under the action of wave trough (Pa) ($d = 62$ cm, $T = 1.26$ s).

H(cm) / z(cm)	3	5	6	7	8	9.8	12	14
0	−45	−87	−93	−106	−124	−160	−188	−200
−3	−40	−68	−80	−93	−114	−139	−171	−187
−7	−32	−56	−66	−74	−101	−128	−153	−177
−10	−23	−43	−48	−61	−86	−101	−144	−169
−15	−24	−42	−46	−60	−78	−88	−134	−140

Under the action of waves, the main forces on the sediment particles on the seabed surface include drag force, lift force, inertia force, underwater friction force, etc. Suspended sediment particles from the seabed surface are mainly subject to gravity, wave seepage force, lift and resistance (particle adhesion, additional pressure of membrane water, etc.). According to Mei and Foda's (1981) boundary layer approximation, the seepage force derived by Xia (2006) is:

$$F = \frac{n}{1-n}\frac{m}{m+1}\frac{\pi d_{50}^3}{6}\frac{\rho_w g H}{2\cosh(kd)}\frac{1}{\delta}\sin\left(kx-\omega t+\frac{\pi}{4}\right) \quad (1)$$

where n is the soil porosity, $m = \frac{nG}{(1-2\nu)\beta}$ is the relative compressibility of water and the soil skeleton, G is the shear modulus, ν is Poisson's ratio, and β is the effective bulk modulus of the pore fluid. d_{50} is the mean particle size of the sediment, ρ_w is the density of water, g is the gravitational acceleration, H is the wave height, k is the wavenumber, d is the

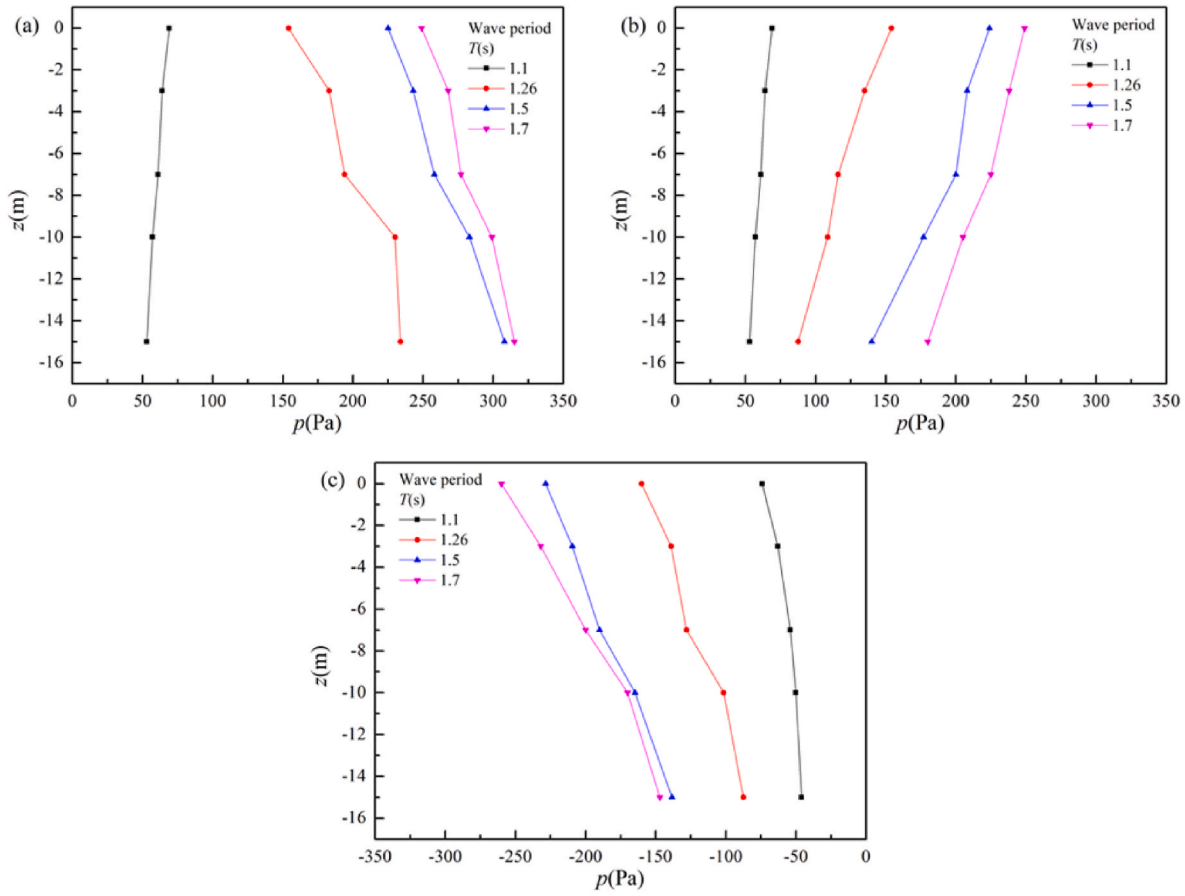

Fig. 16. Variation in pore water pressure amplitude with wave period at different depths in the seabed (a) Amplitude under the wave crest at the maximum accumulated pore water pressure. (b) Amplitude of pore water pressure under the wave crest after 60 min of wave action. (c) Minimum pore water pressure under the wave trough.

Table 5
Maximum pore water pressure under the wave crest at different depths in the seabed at the initial stage of wave action (Pa) ($d = 62$ cm, $H = 9.8$ cm).

T(s) / z(cm)	1.1	1.26	1.5	1.7
0	69	154	225	249
−3	64	183	243	268
−7	61	194	258	277
−10	57	230	283	299
−15	53	234	308	315

Table 6
Maximum pore water pressure under the wave crest at different depths in the seabed after 60 min of wave action (Pa) ($d = 62$ cm, $H = 9.8$ cm).

T(s) / z(cm)	1.1	1.26	1.5	1.7
0	69	154	224	249
−3	64	135	208	238
−7	61	116	200	225
−10	57	109	177	205
−15	53	88	140	180

water depth. δ is the thickness of the seabed boundary layer (Mei and Foda, 1981), $\frac{1}{\delta} = \sqrt{\frac{k_d}{\omega}} / \sqrt{\frac{n}{\beta} + \frac{1}{G}\frac{1-2v}{1-v}}$, $k_d = \frac{k_s}{\rho_w g}$, k_s is the soil permeability in m/sec, and ω is the wave frequency. Before the occurrence of

Table 7
Minimum pore water pressure at different depths in the seabed under the action of the wave trough (Pa) ($d = 62$ cm, $H = 9.8$ cm).

T(s) / z(cm)	1.1	1.26	1.5	1.7
0	−74	−160	−228	−260
−3	−63	−139	−209	−232
−7	−54	−128	−190	−200
−10	−50	−102	−165	−170
−15	−46	−88	−138	−147

Table 8
Suspended sediment concentration under wave action at each wave height ($d = 62$ cm, $T = 1.26$ s).

H(cm)	3	5	6	7	8	9.8	12	14
C(kg/m^3)	0.0	0.0	0.07	0.10	0.12	0.3	0.37	0.53

liquefaction, the pore water pressure decays along the depth, and the seepage force is downward under the action of the wave crest and upward under the action of the wave trough. When the seepage force is upward, the upward force of sediment increases, and the sediment is easier to hang (Myrhaug et al., 2014), which promotes seabed scour, and when the seepage force is downward, it inhibits the hanging of sediment. When the accumulated pore pressure in the seabed is greater than the initial effective stress (Sumer et al., 2012), the seabed liquefies, and it is known from the above that the accumulated pore water pressure

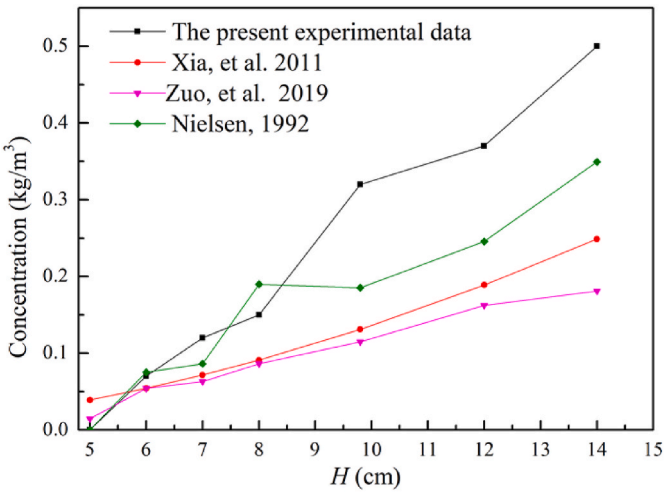

Fig. 17. Suspended sediment concentration under wave action at each wave height (d = 62 cm, T = 1.26 s).

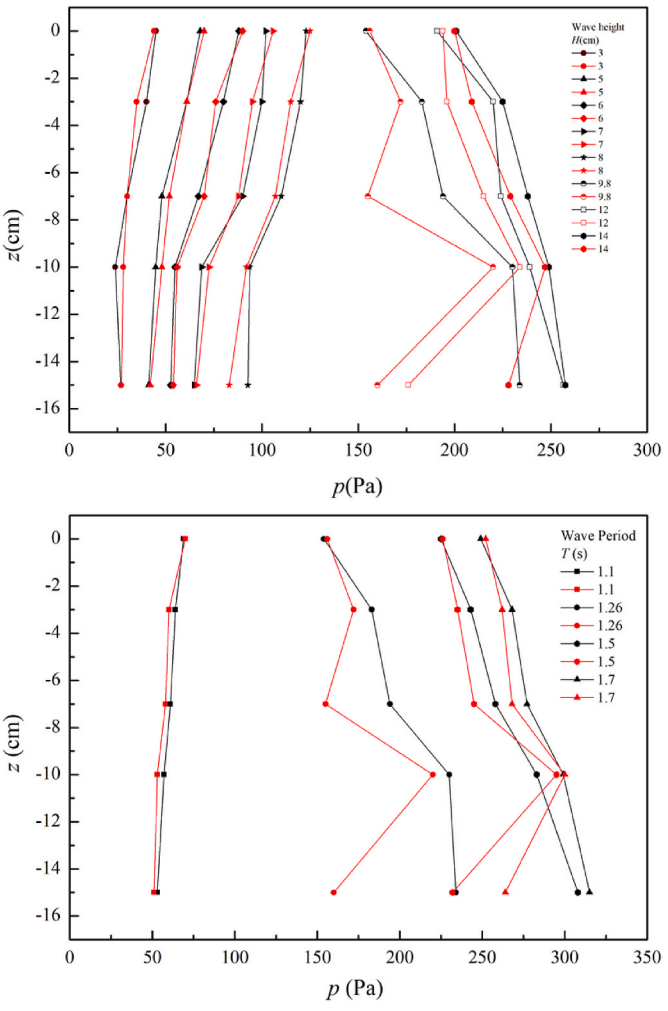

Fig. 18. Amplitude of pore water pressure in the seabed under wave action at each wave height and wave period before and after scour prevention. The black lines are the results with bed scour and the red lines are the results without bed scour. (For interpretation of the references to colour in this figure legend, the reader is referred to the Web version of this article.)

increases along the depth; thus, the vertical gradient of the accumulated pore pressure is generated with time (Guo et al., 2018). This gradient is always upward, which has a continuous upward force on the sediment. At the same time, after seabed liquefaction, the cohesive force between soil particles dissipates, the hindered force of sediment particles decreases, and fine particles are continuously pumped (Tang et al., 2021) from the inside of the seabed to the bed surface, forming a continuous suspension of fine particles, resulting in a significant increase in the near-bottom suspended sediment concentration compared with that before liquefaction. With the increase in wave loading times, the porosity of the seabed decreases gradually, and the gradient of the accumulated pore pressure decreases to less than the initial value. After liquefaction, the sediment receives the continuous upward force induced by the gradient of the accumulated pore pressure, increasing the suspended sediment concentration near the bottom and, thus, intensifying the seabed scour.

4. Dynamic seabed response after erosion prevention

After laying the geotextile, the sand bed was prepared again for testing. In the tests, there was no sediment incipient on the seabed surface, and the suspended sediment concentration near the bottom was zero. In Cases 6–8 and Case 10, Case 11, the seabed was liquefied. At the initial stage of wave loading, liquefaction developed downward, and the maximum liquefaction depth were 11 cm, 12 cm, 12.5 cm, 11 cm, and 12 cm, respectively, which occurred 3 min after wave loading (approximately 150 waves). After 60 min of wave loading, the seabed was dense, and the compression height was approximately 0.5 cm, which was smaller than the existing value of scour. After erosion prevention, the maximum liquefaction depth of the seabed decreased, and the development rate of liquefaction depth slowed down. The variation in pore water pressure amplitude in seabed wave action at each wave height and wave period is shown in Fig. 18, Table 9 and Table 10. The black and red lines in the figure show the pore water pressure amplitude at each depth in the seabed when the bed surface was scoured and the anti-scour measures were settled, respectively.

Under the action of wavelets, bed erosion was not obvious, and the pore water pressure at various depths in the seabed was basically unchanged before and after erosion prevention. However, after the occurrence of seabed liquefaction, the continuous upward force induced by the gradient of the accumulated pore pressure led to a sharp increase in the concentration of suspended sediment near the bottom and obvious bed erosion. After anti-erosion, the amplitude of the pore water pressure in the seabed decreased by approximately 5%–20%. During the coupled action of scour and liquefaction, in Case 6-Case 8, the pore pressure amplitude increased with depth to a depth of 15 cm of the seabed. In combination with Fig. 15, the excess pore water pressure here was greater than the initial effective stress, and the seabed was liquefied. After anti-scouring, the pore water pressure amplitude at a depth of 15 cm was lower than that at a depth of 10 cm. At the same time, according to the liquefaction criteria, the seabed at 10 cm was in the state of liquefaction, but the seabed at a depth of 15 cm was no longer liquefied. The existence of bed scour affects the dynamic response of the seabed and significantly promotes liquefaction.

When the seabed surface is scoured, the sediment particles are suspended and continuously removed, leading to stress release within the soil (Li et al., 2019). The cohesive force between sediment particles decreases, further affecting the initial stress state of the seabed, the pore water pressure in the seabed and intensifying seabed liquefaction.

5. Discussions

The results show that liquefaction and scour promote each other. The coupling mechanism can be explained as follows: when the seabed is scoured, the sediment particles are suspended and removed, leading to stress release in the soil (Li et al., 2019), further affecting the initial

Table 9
Proportion of amplitude decrease of pore water pressure in seabed under wave action at each wave height after erosion prevention (%) ($d = 62$ cm, $T = 1.26$ s).

H(cm) / z(cm)	3	5	6	7	8	9.8	12	14
0	2.27	−2.86	−2.22	−3.60	−1.60	−1.28	−1.55	0.50
−3	14.29	0.00	5.26	5.26	4.35	6.40	12.24	7.66
−7	0.00	−7.69	−4.29	2.52	2.80	25.16	4.19	3.93
−10	−14.63	−6.63	−2.18	−5.38	1.77	4.55	2.15	0.81
−15	−0.81	−1.90	−2.72	−1.62	11.69	46.13	45.72	12.94

Table 10
Proportion of amplitude decrease of pore water pressure in seabed under wave action at each wave period after erosion prevention (%) ($d = 62$ cm, $H = 9.8$ cm).

T(s) / z(cm)	1.1	1.26	1.5	1.7
0	−1.45	−1.30	−0.44	−1.20
−3	6.25	6.01	3.29	2.24
−7	4.92	20.10	5.04	3.25
−10	7.02	4.35	−4.24	−0.33
−15	3.77	31.62	24.68	16.19

stress state of the seabed and intensifying seabed liquefaction. After liquefaction of the seabed, the sediment particles receive a continuous upward force induced by the gradient of the accumulated pore pressure, and the suspended sediment concentration near the bottom is increased, which intensifies the scour of the seabed.

The dynamic response of the seabed under waves is affected by the coupling of liquefaction and scour (Zhang et al., 2020; Tang et al., 2021; Zhai et al., 2021). For example, under a wave height of 9.8 cm, the seabed undergoes a series of processes, such as liquefaction, scour, liquefaction intensification and seabed compaction. At the beginning, the pore water pressure accumulates rapidly and increases along the depth direction, the upward force gradient in the seabed increases, the bonding force between soil particles dissipates, the effective stress is zero, and the seabed is liquefied under waves. Then, the concentration of suspended sediment near the bottom increases, and the sediment particles are continuously removed. Tang et al. (2021) conducted an experiment on the silty seabed in the Yellow River Delta and concluded that seepage failure could "pump" the sediments vertically from the interior of the seabed with a contribution to sediment resuspension of up to 93.2–96.8%. Zhai et al. (2021) considered that small seepage could cause significant changes in the hydrodynamic gradient and further enhance the incipient sediment motion and scour. In the second stage, the excess pore pressure increases further, and the upward force gradient increases, then the seabed liquefaction depth increases. Furthermore, the scour of the seabed is also intensified. Guo et al. (2018) concluded that the vertical gradient of excess pore pressure (seepage force) had a significant effect on sediment transport around the pipeline. In the third stage, with the increase in wave loading times, the seabed in the liquefaction area vibrates periodically with the waves, and the pore water in the seabed is discharged. At this time, the fine particles in the seabed float, the coarse particles sink, and the seabed is reconstructed for the second time. The soil particles are arranged more densely, the porosity of the seabed is reduced, and the liquefaction depth of the seabed is gradually reduced. The fine particle suspension is removed, the seabed is mainly composed of coarse particles, so the concentration of suspended sediment near the bottom is also reduced and the seabed begins to consolidate. In the fourth stage, after the compaction process, the seabed is no longer liquefied, the seepage force under the action of the wave crest is downward, and under the trough is upward, the average pore pressure gradient is reduced, the concentration of suspended sediment near the bottom is lower than that in the liquefaction stage, and the scour of the seabed slows down. The seabed is relatively stable.

6. Conclusion

Seabed dynamic response under waves involves multiple factors, such as erosion, liquefaction, and other phenomena. Experiments on the wave-induced dynamic response in a silty seabed were investigated to reveal the coupling mechanism of scour and liquefaction of the seabed under waves. The geotextile was set on the bed surface to remove the scour disturbance.

Dynamic response experiments of light sandy seabed under waves without geotextile covering with various wave heights and periods were conducted in the wave flume. When the wave height increased, the seabed experienced sand ripples, ripples attenuation, sheet flow and seabed liquefaction. Furthermore, the phase lag after liquefaction was greater than that before liquefaction, and the phase lag inside the liquefaction area also increased with depth. The higher the wave height was, the more obvious the compaction effect and the smaller the phase lag. The influence of periods on the phase lag in the seabed was smaller than that of wave heights. After liquefaction, the suspended sediment concentration increased sharply, which means that liquefaction promoted seabed scour.

When the seabed was covered with geotextile to prevent scour, the concentration of suspended sediment near the bottom of the seabed was zero. The maximum liquefaction depth was reduced by approximately 30%, and the time required to reach the maximum liquefaction depth was reduced by approximately 25%. The amplitude of the pore water pressure in the seabed decreased by approximately 5%–20%. In addition, the pore pressure gradient in the seabed decreased and seabed liquefaction was reduced.

In summary, liquefaction and scouring promote each other.

This study focused on the wave-induced response on the seabed without marine structures. The liquefaction and scouring process of the seabed around the structure under the action of waves has a significant impact on the stability of the structures. In the future, the dynamic response of silty seabeds around structures under wave action should be further studied.

CRediT authorship contribution statement

Lihua Wang: Experiment design, Experiment executor, data collection, Formal analysis, writing, reviewing, and editing. **Jinfeng Zhang:** Experiment design and reviewing, Funding acquisition, Project administration. **Dong-Sheng Jeng:** Experiment design, reviewing and editing. **Qinghe Zhang:** Experiment design, reviewing, and editing. **Tongqing Chen:** Experiment design, reviewing, and editing.

Declaration of competing interest

The authors declare that they have no known competing financial interests or personal relationships that could have appeared to influence the work reported in this paper.

Data availability

Data will be made available on request.

Acknowledgments

This study was supported by the National Natural Science Foundation of China (Grant Nos. 51979190, U1906231), the National Key Research and Development Program of China (Grant No.2021YFB2601100).

References

Chung, S.G., Kim, S.K., Kang, Y.J., Im, J.C., Prasad, K.N., 2006. Failure of a breakwater founded on a thick normally consolidated clay layer. Geotechnique 56 (6), 393–409.
Cubrinovski, M., Bradley, B., Wotherspoon, L., Green, R., Bray, J., Wood, C., Pender, M., Allen, J., Bradshaw, A., Rix, G., Taylor, M., Robinson, K., Henderson, D., Giorgini, S., Ma, K., Winkley, A., Zupan, J., O'Rourke, T., DePascale, G., Wells, D., 2011. Geotechnical aspects of the 22 February 2011 Christchurch earthquake. Bull. N. Z. Soc. Earthq. Eng. 44 (4), 205–226.
Ding, H.Y., Guo, W.B., Zhang, P.Y., Le, C.H., 2013. Response of large-scale bucket foundation used in offshore wind turbine in shoal areas under wind load. J. Tianjin Univ. 46 (2), 121–126.
Dong, J., Xu, J., Li, G., Li, A., Zhang, S., Niu, J., Xu, X., 2022. Experimental study on silty seabed liquefaction and its impact on sediment resuspension by random waves. J. Mar. Sci. Eng. 10 (3), 437.
Gobbi, S., Santisi d'Avila, M.P., Lenti, L., Semblat, J.-F., Reiffsteck, P., 2022. Liquefaction assessment of silty sands: experimental characterization and numerical calibration. Soil Dynam. Earthq. Eng. 159, 107349.
Guo, Z., Jeng, D.-S., Zhao, H., Guo, W., Wang, L., 2018. Effect of seepage flow on sediment incipient motion around a free spanning pipeline. Coast. Eng. 143, 50–62.
Hu, R., Yu, P., Wang, Z., Shi, W., 2020. Pore pressure response and residual liquefaction of two-layer silty seabed under standing waves. Ocean Eng. 218, 108176.
Jeng, D.S., 1997. Wave-induced seabed instability in front of a breakwater. Ocean Eng. 24 (10), 887–917.
Jeng, D.S., Seymour, B.R., 2007. Simplified analytical approximation for pore-water pressure buildup in marine sediments. J. Waterw. Port, Coast. Ocean Eng. 133 (4), 309–312.
Kirca, V.S.O., Sumer, B., Fredsøe, J., 2013. Residual liquefaction of seabed under standing waves. J. Waterway Port Coastal Ocean Eng. ASCE 139, 489–501.
Li, A., Luo, X., Lin, L., Ye, Q., Le, C., 2014. An experimental study on the wave-induced pore water pressure change and relative influencing factors in the silty seabed. J. Ocean Univ. China 13 (6), 911–916.
Le B., Méhauté, 1976. An Introduction to Hydrodynamics and Water Waves. Springer, Berlin/Heidelberg, Germany.
Li, C.-F., Gao, F.-P., 2022. Characterization of spatio-temporal distributions of wave-induced pore pressure in a non-cohesive seabed: amplitude-attenuation and phase-lag. Ocean Eng. 253.
Li, H., Wang, S., Chen, X., Hu, C., Liu, J., 2019. Numerical study of scour depth effect on wave-induced seabed response and liquefaction around a pipeline. Mar. Georesour. Geotechnol. 39 (2), 188–199.
Li, C.-F., Wang, Y., Gao, F.-P., 2022. Spatiotemporal evolution of excess pore pressures in a silty seabed under progressive waves during residual liquefaction. Applied Ocean Research 129, 103401.
Liu, B., Jeng, D.-S., 2015. Laboratory Study for Influence of Clay Content (CC) on wave-induced liquefaction in marine sediments. Marine Georesources & Geotechnology 34, 150429064943006.
Mansard, E.P.D., Funke, E.R., 1980. The measurement of incident and reflected spectra using a least squares method. Coast. Eng. Proc. 1, 8.
Mei, C.C., Foda, M.A., 1981. Wave-induced responses in a fluid-filled poro-elastic solid with a free surface-a boundary layer theory. Geophys. J. Int. 66 (3), 597–631.
Myrhaug, D., Holmedal, L.E., Ong, M., 2014. Seepage effects on bedload sediment transport rate by random waves. Ocean Eng. 82, 123–127.
Nielsen, P., 1992. Coastal bottom boundary layers and sediment transport. Singapore: World Scientific.
Okusa, S., 1985. Wave-induced stresses in unsaturated submarine sediments. Geotechnique 35, 517–532.
Peng, X., Jeng, D.-S., Chen, L.H., Liao, C.C., Yang, H.Q., 2017. Effects of cross-correlated multiple spatially random soil properties on wave-induced oscillatory seabed response. Appl. Ocean Res. 62, 57–69.
Puzrin, A.M., Alonso, E.E., Pinyol, N.M., 2010. Caisson failure induced by liquefaction: Barcelona Harbour, Spain. In: Geomechanics of Failures. Springer, Dordrecht, pp. 85–148.
Qi, W.-G., Gao, F.-P., 2014. Physical modeling of local scour development around a large-diameter monopile in combined waves and current. Coast. Eng. 83, 72–81.
Ren, Y., Xu, G., Xingbei, X., Zhao, T., Wang, X., 2020. The initial wave induced failure of silty seabed: liquefaction or shear failure. Ocean Eng. 200, 106990.
Sumer, B.M., Fredsøe, J., Christensen, S., Lind, M.T., 1999. Sinking/floatation of pipelines and other objects in liquefied soil under waves. Coast. Eng. 38 (2), 53–90.
Sumer, B., Dixen, F., Fredsøe, J., Sumer, S., 2006. The sequence of sediment behaviour during wave-induced liquefaction. Sedimentology 53, 611–629.
Sumer, B., Kirca, V.S.O., Fredsøe, J., 2012. Experimental validation of a mathematical model for seabed liquefaction under waves. Int. J. Offshore Polar Eng. 22, 133–141.
Sui, T., Kirca, V.S.O., Sumer, B.M., Carstensen, S., Fuhrman., D.R., 2022. Wave-induced liquefaction in a silt and seashell mixture. Coast. Eng. 178, 104215.
Sumer, B.M., 2014. Liquefaction Around Marine Structures. World Scientific, New Jersey.
Takegawa, N., Yutaka, S., Murai, K., Kawabata, T., 2016. Influence of liquefaction on scour behind coastal dikes due to tsunami overflow. Int. J. Geotech. Eng. 12, 1–6.
Tang, M., Jia, Y., Zhang, S., Wang, C., Liu, H., 2021. Impacts of consolidation time on the critical hydraulic gradient of newly deposited silty seabed in the Yellow River Delta. J. Mar. Sci. Eng. 9 (3), 270.
Tong, L., Zhang, J., Sun, K., Guo, Y., Zheng, J., Jeng, D.-S., 2018. Experimental study on soil response and wave attenuation in a silt bed. Ocean Eng. 160, 105–118.
Wen, M.-Z., Jia, Y.-G., Wang, Z.-H., Zhang, S.-T., Shan, H.-X., 2020. Wave flume experiments on dynamics of the bottom boundary layer in silty seabed. Acta Oceanol. Sin. 39, 96–104.
Xia, Ling, 2006. Sediment Threshold and Local Scour Around Submarine Pipelines under Wave Action. In: PhD Thesis. Zhejiang University (in Chinese).
Xia, Y.F., Xu, H., Chen, Z., Wu, D.W., Zhang, S.Z., 2011. Experimental study on suspended sediment concentration and its vertical distribution under spilling breaking wave actions in silty coast. China Ocean Eng. 25.
Xu, J., Dong, J., Zhang, S., Sun, H., Niu, J., Li, A., Dong., P., 2022. Pore-water pressure response of a silty seabed to random wave action: Importance of low-frequency waves. Coast. Eng. 178, 104214.
Xu, X., Xu, G., Yang, J., Xu, Z., Ren, Y., 2021. Field observation of the wave-induced pore pressure response in a silty soil seabed. Geo Mar. Lett. 41.
Zhai, H., Jeng, D.-S., Guo, Z., Liang, Z., 2021. Impact of two-dimensional seepage flow on sediment incipient motion under waves. Appl. Ocean Res. 108, 102510.
Zhang, S.-T., Jia, Y.-G., Wang, Z.-H., Wen, M.-Z., Lu, F., Zhang, Y.-Q., Liu, X.-L., Shan, H.-X., 2018. Wave flume experiments on the contribution of seabed fluidization to sediment resuspension. Acta Oceanol. Sin. 37 (3), 80–87.
Zhang, S., Jia, Y., Lu, F., Zhang, Y., Zhang, S., Peng, Z., 2020. Effects of upward seepage on the resuspension of consolidated silty sediments in the Yellow River Delta. J. Coast Res. 36 (2), 372–381.
Zuo, L., Roelvink, D., Lu, Y., 2019. The mean suspended sediment concentration profile of silty sediments under wave-dominant conditions. Continent. Shelf Res. 186, 111–126.